IEEE Access
Multidisciplinary | Rapid Review | Open Access Journal

Received September 1, 2019, accepted September 15, 2019, date of publication September 23, 2019,
date of current version October 7, 2019.

Digital Object Identifier 10.1109/ACCESS.2019.2942738

Digital Sliding Mode Control via a Novel Reaching Law and Application in Shipborne Electro-Optical Systems

JIANQIANG ZHANG[1,2], YONGKAI LIU[1,2], FENGJING ZHANG[3], SHIJIE GAO[1], AND CHENGSHAN HAN[1]

[1]Changchun Institute of Optics, Fine Mechanics and Physics, Chinese Academy of Sciences, Changchun 130033, China
[2]University of Chinese Academy of Sciences, Beijing 100049, China
[3]Aviation University of Air Force, Changchun 130022, China

Corresponding author: Yongkai Liu (liuyk@ciomp.ac.cn)

This work was supported in part by the Research Project of Scientific Research Equipment of Chinese Academy of Sciences (2017), and in part by the Changchun Institute of Optics, Fine Mechanics and Physics, Chinese Academy of Sciences (CIOMP)-Fudan University Joint Fund under Grant Y8O732E.

ABSTRACT The alignment accuracy and stability of shipborne electro-optical system are affected by external attitude disturbance and internal non-linear disturbance. Therefore, this study examined a new digital sliding mode control based on a novel reaching law with an n-order disturbance compensator to solve this problem. Specially, the proposed novel reaching law was a chatter-free method, in which, as the switching gain was replaced by an adaptive function, chattering on the sliding surface tended to zero. For perturbed systems, the new sliding mode controller was able to guarantee a narrow quasi-sliding-mode domain and the ultimate width was the order of $O(T^3)$, such that the narrower the quasi-sliding-mode domain width was, the more robust toward nonlinear disturbances. Both mathematical calculations and simulations verified the convergence and stability of the new controller. Finally, based on a compound control strategy that combined feedforward control with a sliding mode control position loop and proportional-integral velocity loop control structure, shipborne equivalent dynamic target tracking experiments were performed. The results, compared with existing controllers, showed that the robustness of the new controller to nonlinear disturbances was stronger and the tracking system accuracy clearly improved, while the influence of sliding mode chattering on the system was avoided.

INDEX TERMS Shipborne electro-optical system, nonlinear disturbance, digital sliding mode control, chattering, reaching law, disturbance compensator, chattering-free, quasi-sliding-mode domain.

I. INTRODUCTION

Electro-optical systems have been widely used in naval vessels for detection and surveillance, aiming and fire control, precision guidance, navigation and guidance, range measurement, optical communication, and optoelectronic countermeasures [1], [2]. Optical axis stability is a necessary condition for high-precision tracking of shipborne electro-optical systems. However, in real environments, shipborne electro-optical systems are affected by movements caused by ocean waves, causing the optical axis to deviate from the origin of target surface. At the same time, a servo turntable is selected as the actuator in a shipborne electro-optical system, and its nonlinear factors, such as unbalanced internal torque, friction, torque ripple, model identification error of control system, and parameter changes, will lead to unstable system operation, which is the main factor affecting control accuracy of system. Therefore, an effective control method is of great practical significance for suppressing nonlinear disturbances in shipborne electro-optical systems.

In existing studies [3]–[5], a feedforward compensator based on inertial sensors has been applied to shipborne electro-optical systems, with the attitude disturbance of the carrier measured and isolated in real time. And meanwhile, proportional-integral-derivative (PID) controllers have been widely used in industrial control systems because of its simple structure and easily set parameters. However, the PID

The associate editor coordinating the review of this manuscript and approving it for publication was Zheng Chen.

controller, consisting of proportional, integral, and differential linear components of the error, cannot guarantee high control accuracy when the electro-optical system is affected by external ocean waves and internal nonlinear disturbances. Sliding mode control (SMC), as an effective approach to a robust control algorithm, is a good solution for nonlinear systems [7]–[10]. Hence, it is noted that the computer implementation of control algorithms has presented great conveniences recently, and has necessitated the application for the SMC strategy to sampled digital systems. However, if applying continuous-time SMC algorithms to discrete-time systems directly that will lead to many problems, such as large chattering amplitude, sample/hold affects, discretization errors, or even instability [12], [13], and [28]. In order to avoid those problems, the digital sliding mode control algorithm was studied here. In addition, the advantage of DSMC was that once the system trajectories arrive at the sliding surface, DSMC was invariable to system parameter variations and external nonlinear disturbances. System trajectories were stabilized at the quasi-sliding-mode domain (QSMD), and the narrower the QSMD width was, the stronger the system robustness to disturbances. Meanwhile, a control system composed of DSMC and feedforward compensation control was able to effectively isolate wave motion, compensate for nonlinear disturbance in the system, and ensure optical axis stability [11].

However, it has been difficult to directly apply DSMC to shipborne electro-optical stabilization systems. Large and high frequency chattering of the controller is caused by high frequency disturbance of sample/hold effects and discretization errors [12]–[15], which affect control accuracy and damage experimental equipment. Therefore, it is necessary to improve the traditional DSMC to suppress chattering and reduce QSMD width to ensure robustness. Until now, a great number of studies regarding DSMC have been performed to solve this problem, have proposed new digital terminal SMC schemes in which chattering is suppressed by designing nonlinear sliding surfaces [16]–[18]. New adaptive time-delay algorithms have been proposed that combined time-delay estimation, injected dynamics and adaptive laws, which is an effective method for suppressing nonlinear disturbances in the system, the time-delay, and chattering on the sliding mode [19]. A novel adaptive fractional-order nonsingular terminal sliding mode has been proposed that combines reaching law (RL) with adaptive technique to obtain fast convergence and high precision and chatter reduction [20]. An adaptive super-twisting fractional-order nonsingular terminal sliding mode control has been proposed, which ensures an algorithm with fast dynamic response and high control accuracy [22]. A roust adaptive second-order SMC with a PID sliding surface has been presented for uncertain linear systems. The discontinuous sign function is used for the time-derivative of the control signal and the chattering reduced [23]. A self-tuning integral sliding mode controller combined with a composite nonlinear feedback law has been designed, which suggested a varying boundary layer width and a variable control gain that successfully eliminates chattering [24]. A novel global sliding mode stabilizer algorithm has been proposed in which chattering on the sliding mode is effectively reduced [25]. High-order sliding mode extends the idea of the traditional sliding mode and the discontinuous control quantity has been applied to the high-order derivative of the sliding mode. This method is able to eliminate chattering while having the advantages of simple structure and strong robustness of the traditional sliding mode algorithm [4], [26]. Among of these studies, the RL is the most direct and effective algorithm to eliminating chattering of sliding mode. The chatter-free method has been discussed, with the signum function canceled or replaced by a continuous function, with chattering in the sliding mode tending to 0 and, for the perturbed system, nonlinear disturbance is suppressed and the difference function also adopted to further narrow the QSMD width, on the order $O(T^3)$ [6], [14], [27], [34], and [35]. The chatter-reduced RL with a disturbance compensator has been applied to uncertain systems, with signum function coefficients replaced by exponential terms that dynamically adapt to variations in switching gain, to ensure less chattering [13], [28]–[31]. For a perturbed system, the QSMD width is the order of $O(T^2)$ and $O(T^3)$ in different studies ([13] and [28], [29] respectively). It is clear that such methods cannot completely eliminate sliding mode chattering, as high frequency chattering still exists in the output. Also, QSMD width methods in other studies are larger than $O(T^3)$, such that the wider QSMD means less robustness to disturbances [6], [14], and [27].

Above all, sliding mode chattering and robustness are the two main problems of sliding mode control systems. Therefore, the main contributions of this study were described below.

1) This paper proposed a novel RL designed by an adaptive function, which was related to state errors, and compared with existing algorithms, such as the ref. [6] and the ref. [13] algorithms. This proposed algorithm solved the chattering problem existing in classical sliding mode control, offering a chatter-free algorithm. Meanwhile, the QSMD width of the proposed algorithm was the order of $O(T^3)$ such that the robust of system was guaranteed. Both mathematical deductions and simulations showed the effectiveness of the proposed algorithm.
2) Shipborne equivalent dynamic target tracking experiments based on sliding mode control were performed and the digital control combined feed-forward control with a SMC position and PI velocity loop control structures were adopted. The results, compared with the PID controller and other existing representational sliding mode controllers such as references [6] and [13], showed that both the sliding mode and PID controllers isolated attitude disturbance, but the tracking error of the proposed method was the least of these approaches. In addition, compared with Ref. [13], the proposed

method avoided the influence of sliding mode chattering on the system.

II. PLANT MODEL AND DESIGNED OF SLIDING MODE

In this chapter, the basic content of the DSMC was discussed, including the shipborne electro-optical system, the discrete-time system model, sliding mode surface, and QSMD width.

A. THE DISCRETE-TIME SYSTEM MODE

Shipborne electro-optical systems are susceptible to nonlinear factors, such as waves, being model uncertainties and, thus, it is difficult to describe a shipborne electro-optical system with an accurate mathematical model. Indeed, the nonlinear model of the control system was expressed by the equation of state, equation (1) [6], [10], and [15], as was the shipborne control system.

$$x(k+1) = (A + \Delta A(k))x(k) + (B + \Delta B(k))u(k) + B_f\rho(k), \tag{1}$$

where $x(k)\epsilon R^{n\times 1}$ is the system state, $u(k)\epsilon R$ the control input, A and B system model parameters with approximate estimation, the matrix A, B controllable, $\Delta A(k)$ and $\Delta B(k)$ the model uncertainties, and $\rho(k)\epsilon R$ the nonlinear disturbance in the system, such as nonlinear disturbances caused by ocean waves and unbalanced system torque.

Assumption 1: According to reference [37], if the uncertainties $\Delta A(k)$, $\Delta B(k)$, and $\rho(k)$ are bounded and satisfy the ''matching'' condition, then it must be satisfied that

$$\varsigma(k) = \Delta A(k)x(k) + \Delta B(k)u(k) + B_f\rho(k), \tag{2}$$

where $\varsigma(k)\epsilon R^{n\times 1}$ represents all uncertainties in the system and its upper bound ς. Thus, the discrete-state equation was expressed as

$$x(k+1) = Ax(k) + Bu(k) + \varsigma(k), \tag{3}$$

Assumption 2: The change rate of the generalized uncertainty is bounded, which means uncertainty is slowly varying with time [6].

B. THE SLIDING SURFACE

In this study, the typical switching function S was adopted, defined as [8]

$$s(k) = C_e e(k) = C_e\,(x(k) - R_n(k)), \tag{4}$$

where $C_e = [C_{e1}, C_{e2}, \ldots, 1]$ is the sliding mode coefficient matrix and $e(k)$ the actual error between the ideal state $R_n(k)$ and real state $x(k)$. Thus, the sliding surface was expressed as

$$S = \{e(k)|C_e e(k) = 0\}. \tag{5}$$

The stability of the sliding mode and the asymptotic rate of approaching movement were in direct with the value of C_e [10].

Lemma 1: The sliding mode coefficient max, $C_e = [C_1, C_2, \ldots, C_{n-1}, 1]\epsilon R^n$ with $C_1, C_2, \ldots, C_{n-1}, 1$, being the positive sliding function gains satisfying the polynomials $\psi(p) = p^{n-1} + C_{n-1}p^{n2} + \ldots + C_2p + C_1$, and must be Hurwitz polynomials. Further details of sliding function gain selection can be found in references [35], and [38].

C. THE QSMD

Definition 1: System (3) would be in a QSM in the Δ (defined below) vicinity of the sliding surface (5), if the states satisfies $\{e(k)|C_e e(k) = 0\}$ for all $k > n$ (n is a constant integer). This specified domain where the QSM occurs is called the QSMD and the positive constant Δ the QSMD width [10], [13], [28], and [33].

Definition 2: The conditions that system (3) satisfies in reaching QSM in the Δ vicinity of the sliding surface (5) are

$$\begin{cases} \text{if } s(k) > \Delta, & -\Delta < s(k+1) < s(k) \\ \text{if } s(k) < -\Delta, & s(k) < s(k+1) < \Delta \\ \text{if } |s(k)| < \Delta, & |s(k+1)| < \Delta. \end{cases} \tag{6}$$

III. THE NEW REACHING LAW

In this chapter, a DSMC controller, based on the new RL with a disturbance compensator, was proposed and its stability demonstrated by analyzing approaching movement and sliding mode in sections ***B*** and ***C***.

A. THE NEW RL WITH A DISTURBANCE COMPENSATOR

Chattering is the main problem of the DSMC, which leads to high frequency disturbances in the system. A new RL, based on an exponential RL, was proposed in this section, which was able to solve the chattering problem by adapting to changes in system trajectories and state errors.

This new RL was given by

$$s(k+1) = (1 - \lambda T)\cdot\Gamma_1(k)\cdot s(k) - \kappa T\cdot\Gamma_2(k)\cdot \mathrm{sgn}[s(k)], \tag{7}$$

where the exponential coefficient was $0 < \lambda T < 1$, the switching gain $\kappa > 0$, and T the sampling time for discrete systems. The adaptive functions in (7) were expressed as

$$\begin{cases} \Gamma_1(k) = \varepsilon + (1-\varepsilon)e^{-2\eta\cdot|s(k)|^{\gamma_1}} \\ \Gamma_2(k) = \dfrac{|e_1(k)|^{\alpha}}{\varepsilon + (1 + |e_1(k)|^{\alpha^1} - \varepsilon)e^{-\eta\cdot|s(k)|^{\gamma_2}}}, \end{cases} \tag{8}$$

where $0 < \varepsilon < 1$, $0 < \gamma_1 < 1$, $\eta > 0$, $\gamma_2 \geq 1$, (η, $\gamma_2\epsilon N_+$), the parameter $e_1(k)$ represented the first element of the error matrix $e_1(k)$ between the measured value $x(k)$ and target value $R_n(k)$ and, if $|e_1(k)| \geq 1$, then $0 < \alpha < 1$; otherwise if $0 \leq |e_1(k)| \leq 1$, then $\alpha > 1$.

Remark 1: These parameters were discussed in *simulation 4.1 case II* below.

Solving (8) based on (3) and (4), the DSMC controller was:

$$u(k) = (C_eB)^{-1}[C_e(R_n(k+1) - Ax(k)) + (1-\lambda T) \cdot\Gamma_1(k)s(k) - \kappa T\cdot\Gamma_2(k)\mathrm{sgn}[s(k)] - C_e\varsigma(k)], \tag{9}$$

in which $\varsigma(k)$ respects the system uncertainties. In view of previous studies [13], [28], and [29], the disturbance was estimated by the delay estimate method, with $\hat{\varsigma}(k)$ in respect

to the estimation, as [29]: $\hat{\varsigma}$ (k) $=$ $\varsigma(k-1)$, and [13], [28] $\hat{\varsigma}(k) = \varsigma(k-1) + \varsigma(k-1) - \varsigma(k-2)$, where $\varsigma(k-1) = x(k) - \mathrm{A}x(k) - \mathrm{B}u(k-1)$.

Based on the above, a new n-order disturbance compensator was proposed here as:

$$\hat{\varsigma}(k) = \varsigma(k-1) + \sum_{i=1}^{n} \alpha_i \cdot [\varsigma(k-i) - \varsigma(k-1-i)]. \quad (10)$$

where α was the error weighting factor, with $\alpha_0 + \alpha_1 + \ldots \alpha_n = 1$, in periodically disturbed signals and the magnitude of the disturbance approximately equal to that of the adjacent time, $\alpha_1 > \alpha_2 > 3 \ldots > \alpha_n$. Its convergence was discussed in Appendix A.

Usually, n was selected to be 2, with the disturbance estimate related to two past disturbance differences. Therefore, the 2nd-order disturbance compensator was

$$\begin{aligned}\hat{\varsigma}(k) &= \varsigma(k-1) + \alpha \cdot [\varsigma(k-1) - \varsigma(k-2)] \\ &\quad + (1-\alpha) \cdot [\varsigma(k-2) - \varsigma(k-3)] \\ &= (1+\alpha)\varsigma(k-1) \\ &\quad + (1-2\alpha)\varsigma(k-2) - (1-\alpha)\varsigma(k-3). \quad (11)\end{aligned}$$

The final DSMC controller was then inferred as:

$$\begin{aligned}u(k) = (C_e B)^{-1}[C_e(R_n(k+1) - Ax(k)) + (1-\lambda T) \\ \cdot \Gamma_1(k)s(k) - \kappa T \cdot \Gamma_2(k)\mathrm{sgn}[s(k)] - C_e\hat{\varsigma}(k)], \quad (12)\end{aligned}$$

and the RL with a disturbance compensator expressed as:

$$s(k+1) = (1-\lambda T)\Gamma_1(k)s(k) - \kappa T \Gamma_2(k)\mathrm{sgn}[s(k)] + \varphi(k), \quad (13)$$

where the error of estimation was

$$\varphi(k) = C_e[\varsigma(k) - \hat{\varsigma}(k)]. \quad (14)$$

Lemma 2: $\varsigma(k) = O(T)$, $\varsigma(k) - \varsigma(k-1) = O(T^2)$, and $\varsigma(k) - 2\varsigma(k-1) + \varsigma(k-2) = O(T^3)$ [13].

According to (11), the estimation error was

$$\begin{aligned}&(1+\alpha)\varsigma(k-1) + (1-2\alpha)\varsigma(k-2) - (1-\alpha)\varsigma(k-3) \\ &\quad = 2\varsigma(k-1) - \varsigma(k-2) - (1-\alpha) \\ &\qquad \cdot \{[\varsigma(k-1) - \varsigma(k-2)] - [\varsigma(k-2) - \varsigma(k-3)]\}, \quad (15)\end{aligned}$$

and because of *Assumption 2*, if the uncertainty was slowly varying with time, it was obtained that

$$\begin{aligned}(1-\alpha)\{&[\varsigma(k-1) - \varsigma(k-2)] \\ &- [\varsigma(k-2) - \varsigma(k-3)]\} \approx 0, \quad (16)\end{aligned}$$

Therefore, in view of *Lemma 2*, it was derived that

$$\begin{aligned}\varphi(k) &= C_e[\varsigma(k) - \hat{\varsigma}(k)] \\ &\approx C_e[\varsigma(k) - 2\varsigma(k-1) + \varsigma(k-2)] \\ &= C_e O(T^3) = O(T^3). \quad (17)\end{aligned}$$

Lemma 2 was needed in the proof of *Theorem 2 (3)*.

In view of previous studies [7], [8], [12], $\Gamma_2(k)$ is related to the state error, which can adjust the coefficient of sgn[$s(k)$] adaptively to guarantee the fast speed of the reaching movement as well as small chattering. Actually, if the state error is large, $|s(k)|$ will be large and the approaching movement will do. In this movement, the exponential coefficient tends to be $(1-\lambda T)\cdot\varepsilon$, which is smaller than $(1-\lambda T)$ and the switching gain tends to be $(\kappa T \cdot |e_1|^{\alpha})/\varepsilon$, which is far greater than κT and a fast speed of the approaching movement can be guaranteed. If the system is in the stage of sliding mode, the state error tends to 0, $|s(k)| \approx 0$, and meanwhile, the switching gain tends to be $(\kappa T \cdot |e_1|^{\alpha})/(1 + \kappa T \cdot |e_1|^{1/\alpha})$, which was much smaller than κT, such that the chattering on the sliding surface was reduced [6].

Remark 2: Analyzing similarly, in view of the algorithmic structure of the chatter-reduced algorithm [13], when the system state was near the sliding surface, the coefficient of the switching function sgn[s(k)] tended to κT, with chattering on the sliding mode still active. Therefore, the proposed algorithm was advanced that chattering on the sliding mode of the proposed algorithm tended to be free.

B. THE APPROACHING MOVEMENT

Theorem 1: Consider that the compensation is bounded, such that the upper bound is φ and ς is the disturbance maximum. If the controller (12) is implemented, then the trajectories of the system from any initial state will first cross the sliding surface (5) within at most $m^* + 1$steps.

Proof: there is an initial state that causes the switching function (4), as $s(0)$, $s(1)$, $s(2)$,. . . and $s(n)$ do not change sign, with n a positive integer. Actually, two cases needed to be considered, for positive and negative values of $s(k)$.

1) If $S(K) \geq 0$ $(K = 0, 1, 2 \ldots N)$ and the system trajectories did not cross the sliding surface in number of steps N, IT was concluded from (4) and (7) that

$$s(1) = (1-\lambda T)\Gamma_1(0) \cdot s(0) - \kappa T \cdot \Gamma_2(0) + \varphi(0) \quad (18)$$

$$\begin{aligned}s(2) &= (1-\lambda T)\Gamma_1(1) \cdot s(1) - \kappa T \cdot \Gamma_2(1) + \varphi(1) \\ &= (1-\lambda T)^2\Gamma_1(0)\Gamma_1(1) \cdot s(0) - (1-\lambda T)\Gamma_1(1) \\ &\quad \cdot (\kappa T \Gamma_2(0) - \varphi(0)) - (\kappa T \cdot \Gamma_2(1) - \varphi(1)) \quad (19)\end{aligned}$$

$$\vdots$$

$$\begin{aligned}s(n) &= (1-\lambda T)^n \prod_{i=0}^{n-1} \Gamma_1(i)s(0) - \sum_{j=0}^{n-2} (1-\lambda T)^{n-1-j} \\ &\quad \cdot [\Gamma_1(n-1) \cdot \cdot \Gamma_1(j+1)] \cdot [\kappa T \Gamma_2(j) - \varphi(j)] \\ &\quad - [\kappa T \Gamma_2(n-1) - \varphi(n-1)] \\ &= (1-\lambda T)^n \chi_1 s(0) - \sum_{j=0}^{n-2} (1-\lambda T)^{n-1-j} \\ &\quad \cdot [\Gamma_1(n-1) \cdot \cdot \Gamma_1(j+1)] \cdot [\kappa T \Gamma_2(j) - \varphi(j)] \\ &\quad - [\kappa T \Gamma_2(n-1) - \varphi(n-1)], \quad (20)\end{aligned}$$

assuming that

$$\chi_1 = \prod_{i=0}^{n-1} \Gamma_1(i). \quad (21)$$

Moreover, in view of (7), it was obtained that $\varepsilon <_1 (k) < 1$, such that χ_2 was effectively defined as:

$$\chi_2 = \min\{\Gamma_1(\text{n-1}) \cdot \cdot \Gamma_1(\text{j+1})\} \leq 1, \text{j} \in N_+. \tag{22}$$

According to equations (20), (21), and (22):

$$\begin{aligned} s(n) &< (1-\lambda T)^n \chi_1 \cdot s(0) - \chi_2 \sum_{j=0}^{n-2} (1-\lambda T)^{n-1-j} \\ &\quad \cdot [\kappa T \Gamma_2(j) - \varphi] - [\kappa T \Gamma_2(n-1) - \varphi] \\ &< (1-\lambda T)^n \chi_1 s(0) \\ &\quad - \chi_2 \sum_{j=0}^{n-1} (1-\lambda T)^{n-1-j} [\kappa T \Gamma_2(j) - \varphi] \end{aligned} \tag{23}$$

And there must be a positive number to satisfy formula (24) as

$$\sum_{j=0}^{n-1} (1-\lambda T)^{n-1-j} [\kappa T \Gamma_2(j) - \varphi(j)] = \sum_{j=0}^{n-1} (1-\lambda T)^{n-1-j} \chi_3, \tag{24}$$

It was easy to reach the conclusion that

$$\chi_3 = \frac{\sum_{j=1}^{n-1} (1-\lambda T)^{n-1-j} \cdot [\kappa T \Gamma_2(j) - \varphi(j)]}{\sum_{j=1}^{n-1} (1-\lambda T)^{n-1-j}}. \tag{25}$$

Therefore, combining (23) with (25), it was able to be implanted that:

$$s(n) < (1-\lambda T)^n \chi_1 s(0) - \chi_2 \chi_3 \sum_{j=0}^{n-1} (1-\lambda T)^{n-1-j}. \tag{26}$$

As this point, supposing that system trajectories arrived at the sliding surface at m, then $s(m) = 0$ and the conclusion followed according to (26)

$$\begin{aligned} s(m) &= (1-\lambda T)^m \chi_1 s(0) - \chi_2 \chi_3 \sum_{j=0}^{m-1} (1-\lambda T)^{m-1-j} \\ &= (1-\lambda T)^m \chi_1 s(0) - \chi_2 \chi_3 \frac{1-(1-\lambda T)^m}{\lambda T}, \end{aligned} \tag{27}$$

and therefore, the system reaching time was expressed as

$$m = \log_{1-\lambda T} \frac{1}{\chi_1 \lambda T \cdot s(0) \big/ \chi_2 \chi_3 + 1}. \tag{28}$$

where coefficient values are as shown by (21), (22), and (25). Here, m^* was assumed to be the maximal integer bounded below the real number m, such that, when $s(k) \geq 0$, system trajectories crossed the sliding mode surface at steps $m^* + 1$.

2) If $S(K) \leq 0$ $(K = 0, 1, 2 \ldots n)$, for all conditions as well as case (a), system trajectories were assumed to arrive at the sliding surface at m and the integer below m is m^*, it can be concluded that

$$m = \log_{1-\lambda T} \frac{1}{-\chi_1 \lambda T \cdot s(0) \big/ \chi_2 \chi_3 + 1}. \tag{29}$$

Thus, when $s(k) \leq 0$, system trajectories crossed the sliding surface at steps $m^* + 1$.

In the two above cases, system trajectories reached the sliding surface in limited time m (shown as (30)) no matter where the initial state was and the reaching steps were m^*+1. After this, it was entered into the QSMD.

$$m = \log_{1-\lambda T} \frac{1}{\chi_1 \lambda T \cdot |s(0)| \big/ \chi_2 \chi_3 + 1}. \tag{30}$$

Theorem 1: Has been proved.

C. STABILITY ANALYSIS OF THE SLIDING MODE

The following results were derived from the analysis of system stability in a discrete-time system (3) in the Δ vicinity of the sliding surface.

Theorem 2: Three conclusions were derived to hold the closed-loop system (3) with controller (12):

1) The system trajectories from any initial state entered into the QSMD, defined by

$$\Phi = \{s(k) \,|\, |s(k)| \leq \Delta_\Phi = \kappa T \Gamma_2 + \varphi\}. \tag{31}$$

where $\varphi/\kappa T \leq \Gamma_2 < 1$, and there must be a positive root satisfying equation $\varphi/\kappa T \leq \Gamma_2(k)$ (proof in Appendix B).

2) Once the system trajectories entered into the QSMD, they could not escape it.

3) Compared to previous algorithms, the proposed RL was able to guarantee a smaller QSMD width.

Proof: there were two cases that needed to be considered as well as the proof of *Theorem 2*, with positive and negative values of $s(k)$.

1) If $s(k) > 0$, it was clear that

$$\begin{aligned} s(k+1) &= (1-\lambda T)\Gamma_1(k) s(k) \\ &\quad - \kappa T \Gamma_2(k) \text{sgn}[s(k)] + \varphi(k) \\ &< s(k) - \kappa T \Gamma_2 + \varphi < s(k). \end{aligned} \tag{32}$$

It was concluded that $s(k)$ was monotonically decreasing with respect to k as long as $s(k)$, such that there must be a positive integer n^* that satisfied:

$$0 < s(n^*) < \kappa T \cdot \Gamma_2 + \varphi. \tag{33}$$

If $s(k) < 0$, it was obtained that

$$\begin{aligned} s(k+1) &= (1-\lambda T)\Gamma_1(k) s(k) \\ &\quad - \kappa T \Gamma_2(k) \text{sgn}[s(k)] + \varphi(k) \\ &> s(k) + \kappa T \cdot \Gamma_2 + \varphi > s(k), \end{aligned} \tag{34}$$

where $s(k)$ was monotonically increasing with respect to k as long as $s(k) < 0$, such that there also must have a positive integer n^* that satisfied

$$-(\kappa T \cdot \Gamma_2 + \varphi) < s(n^*) < 0. \tag{35}$$

Therefore, on the basis of (33) and (35), the following conclusion was:

$$\left|s(n^*)\right| < \kappa T \cdot \Gamma_2 + \varphi. \tag{36}$$

Of the above, system trajectories from any initial state must enter into the QSMD, defined by (31).

Theorem 2 (1): Has been proven.

2) Assume system trajectories have entered into the QSMD, such that, if $0 < s(k) < \kappa T \cdot \Gamma_2 + \varphi$, $\Gamma_1(k) \sim 1$, $\Gamma_2(k) \leq \Gamma_2$, and $\varphi(k) \leq \varphi$, then

$$\begin{aligned} s(k+1) &= (1-\lambda T)\Gamma_1(k)s(k) \\ &\quad -\kappa T\Gamma_2(k)\mathrm{sgn}[s(k)] + \varphi(k) \\ &< s(k) - \kappa T\Gamma_2 + \varphi < s(k) < \kappa T \cdot \Gamma_2 + \varphi, \end{aligned} \tag{37}$$

when $-\kappa T \cdot \Gamma_2 - \varphi < s(k) < 0, \Gamma_1(k) \sim 1, \Gamma_2(k) \leq \Gamma_2$, and $\varphi(k) \leq \varphi$, it was obtained that:

$$\begin{aligned} s(k+1) &= (1-\lambda T)\Gamma_1(k)s(k) \\ &\quad -\kappa T\Gamma_2(k)\mathrm{sgn}[s(k)] + \varphi(k) \\ &> s(k) + \kappa T\Gamma_2(k) + \varphi(k) \\ &> s(k) > -\kappa T \cdot \Gamma_2 - \varphi. \end{aligned} \tag{38}$$

The conclusion from (36) and (37) was that if system trajectories $s(k)$ have been in the QSMD, the next step $s(k+1)$ must belong to it or, in other words, once the system trajectories entered into the QSMD, they could not escape it.

Theorem 2 (2): Has been proven.

Proof: According to (30), the width of QSMD Δ_Φ was related to the upper bound of the disturbance estimation error $\varphi(k)$. In view of *Lemma 2* and (17), it was derived that

$$\Delta_\Phi = \kappa T\Gamma_2 + \varphi = O(T^3) + O(T^3) = O(T^3). \tag{39}$$

In view of [6], [29], the width was the order of magnitude $O(T^2)$, and therefore, the QSMD width based on the proposed method were smaller, having the magnitude order of $O(T^3)$.

Theorem 2 (3): Has been proven.

Remark 3: in view of algorithmic structure of the chatter-free algorithm Ref. [6], the width of QSMD tended to the order of $O(T^2)$, which was much wider than that of the proposed algorithm; the wider the QSMD width was, the worse the system robustness. Therefore, the proposed algorithm possessed advantages.

Remark 4: the parameters of the RL (13) were general to the different models, and meanwhile, they did not affect the width Δ_Φ, which only affected the chattering of the transition stage of approaching motion and sliding mode only (*simulation 4.1 case II*).

D. SUMMARY

From *theorem 1* and *2*, it was obvious that the DSMC controller (12), based on the RL (13) was convergent and stable. System trajectories must arrive at the sliding surface in a limited time no matter where the initial state was. Here, the sliding mode chattering was effectively suppressed and the QSMD width perforce smaller than the method [13]. For both the approaching movement and the sliding mode, the system trajectories based on the RL are shown in Figure.1.

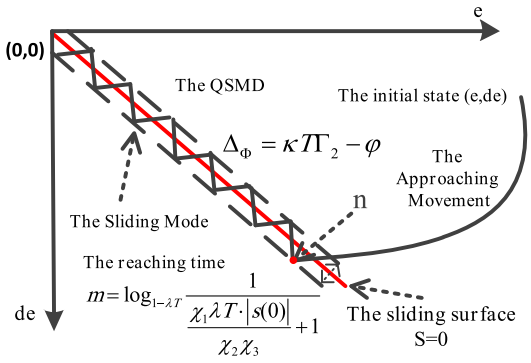

FIGURE 1. System trajectories of the proposed RL.

IV. SIMULATIONS RESULTS AND ANALYSIS

According to equation (1) and supposing the discrete time digital system with nonlinear disturbance was expressed as

$$\begin{aligned} x(k+1) &= (A + \Delta A(k))x(k) + (B + \Delta B(k))u(k) + B_f\rho(k) \\ A &= \begin{bmatrix} 1 & 0.0088 \\ 0 & 0.7788 \end{bmatrix}, \quad B = \begin{bmatrix} 0.0061 \\ 1.1768 \end{bmatrix}, \\ B_f\rho(k) &= \begin{bmatrix} 0 \\ f(k) \end{bmatrix} \\ \Delta A(k) &= \beta \cdot \begin{bmatrix} 0 & 0 \\ 0 & 0.5\sin(\pi k) \end{bmatrix}, \\ \Delta B(k) &= \beta \cdot \begin{bmatrix} 0 \\ 0.5\sin(\pi k) \end{bmatrix} \\ f(k) &= \beta \cdot [0.5 + 2.5\sin(2\pi k) + 0.5\cos(0.5\pi k)], \end{aligned} \tag{40}$$

where the initial state was assumed that $[-0.8; -0.5]$.

According to *Lemma 1*, the order of system was 2 and, therefore, the sliding mode coefficient matrix of the switching function (4) was $[C_1, 1]$, which satisfied the Hurwitz polynomials, with the eigenvalues of the polynomials $p + C_1 = 0$ negative, with $C_1 > 0$. The switching function (4) parameter chosen as $C_e = [5, 1]$.

In the next sections, two simulations were compared with existing studies. First, no disturbance was supposed in the system and analyzed chattering on the sliding mode. And second, assuming the nonlinear disturbance in the system, the performance of sliding mode controller analyzed, and the QSMD width discussed.

Matlab, as an effective simulation tool, was used to analyze the performance of the proposed algorithm, Ref. [6] and [13] algorithms.

A. CHATTERING ANALYSIS

Case I: Assuming no disturbance in system (41) and with the adjustable parameter $\beta = 0$, the exponential coefficient was selected as $\lambda = 5$, the big switching gain $\kappa = 5$, the coefficients of nonlinear function selected as $\varepsilon = 0.15$, $\eta = 20$, $\gamma_1 = 0.5$, $\gamma_2 = 10$, when $|e_1| \geq 1$, $a = 2$. These parameters were selected to guarantee an implemented system. Coefficients of [13] were same as the above and system trajectories shown in Figure 2.

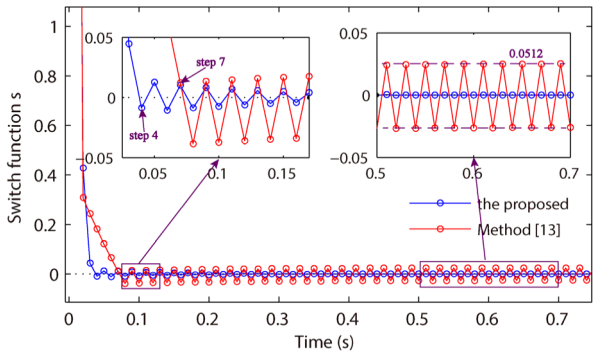

FIGURE 2. System trajectories based on the RL.

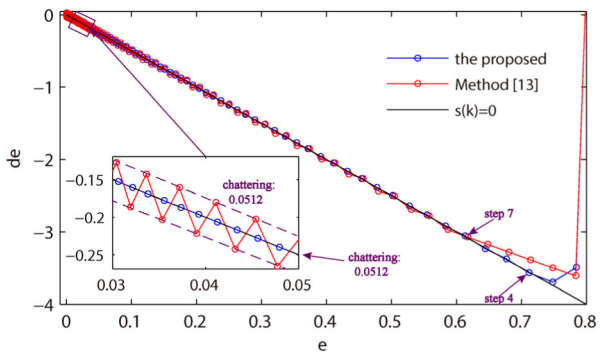

FIGURE 3. Phase trajectories of sliding mode movement.

In view of the Figures 3 and 4, initially, some conclusions were drawn:

1) In the initial stage, system states of both methods were far away from the sliding surface, $|e_1| \approx \infty$, with the trajectories of both systems in the approaching movement. Once trajectories were close to the sliding surface, they were stabilized at the QSMD;
2) system trajectories in the proposed RL first crossed the sliding surface in $k_1 = 4$ and its convergence rate was three steps faster than the method [13], $k_1 = 7$;
3) chattering on the sliding surface of the proposed RL was close to 0, which was far smaller than that of method [13], almost 5.12×10^{-2};
4) because of no disturbance, the QSMD width was equal to chattering on the sliding surface.

Therefore, the proposed method was able to solve the chattering problem of the sliding mode

Case II: In equations (7) and (8), many parameters affected the system. How those parameters affected trajectories was discussed necessary, however, it is difficult to calculate the exact interval of parameter selection because the approximate equalities (21), (22), and (25). Therefore, range of parameters found for minimum chattering and a fast rate of approaching movement examined in the following simulation.

From comparisons of system trajectories with different values of ε, γ_1, λ, and α respectively, it was obvious that parameters were related to the approaching movement and the chattering on the surface tended to 0 whatever those

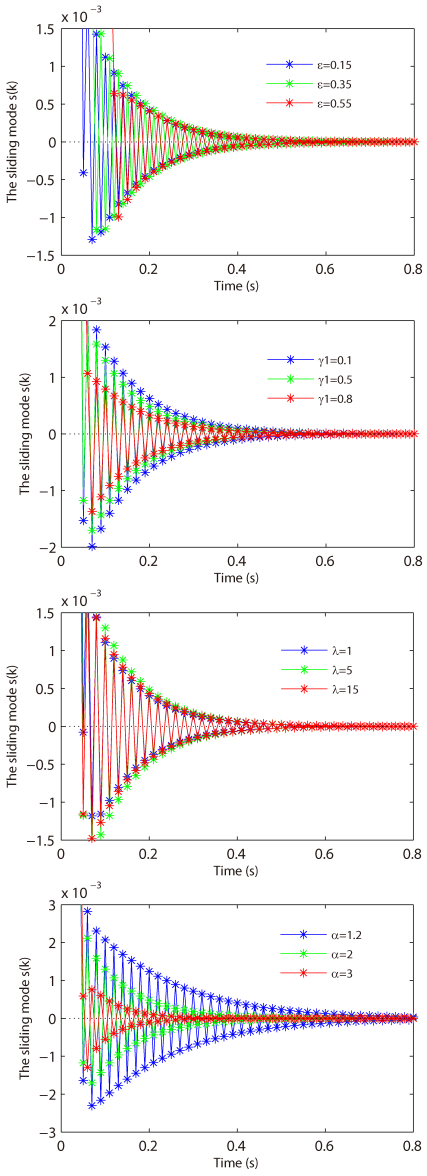

FIGURE 4. System trajectories with different values of ε, γ_1, λ, and α.

parameters (ε, γ_1, λ, and α) were selected (Fig. 4). The bigger ε, γ_1, λ, and α were and the smaller ε was, the faster the approaching rate as well as the smaller the chattering of the transition stage from approaching motion to the sliding mode. Meanwhile, η and γ_2, as coefficients of the exponential $|s(k)|$, did not affect the chattering. As usual, those parameters were selected, such that $\varepsilon = 0.15$, $\gamma_1 = 0.1$, $\lambda = 5$, $\alpha = 2$, $\eta = 20$ and $\gamma_2 = 10$. The switching gain κT related to the maximum disturbance estimation error, which was selected in the next section.

B. QSMD ANALYSIS

For comparison, three kinds of methods were employed.

Case I: Supposing the system (41) with nonlinear disturbance, the adjustable parameter $\beta = 1$ and, in view of (11) and (14), the error of disturbance estimation is shown in Figure 5, where the error weighting factor was $\alpha = 0.95$.

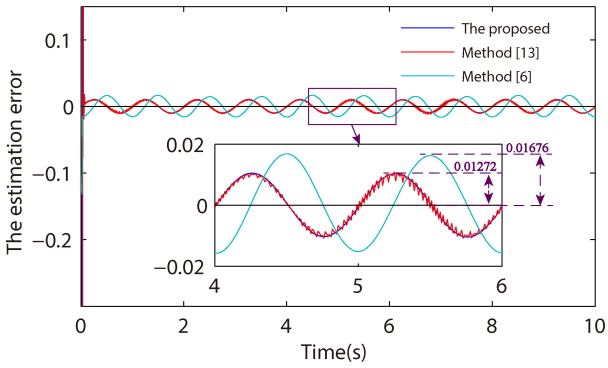

FIGURE 5. Disturbance estimate error.

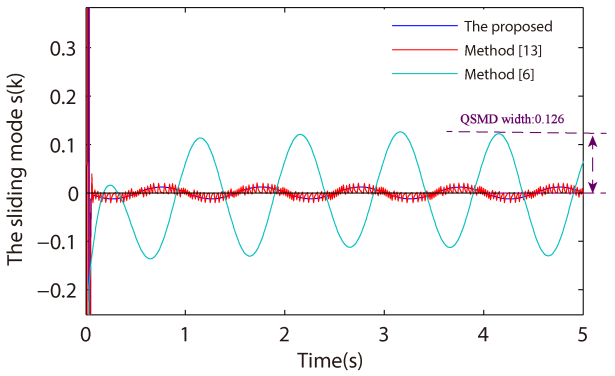

FIGURE 6. System trajectories based on the RL.

TABLE 1. Parameters of the three algorithms.

Parameters	Proposed	Ref.[13]	Ref.[6]
Sliding matrix	[5,1]	[5,1]	[0.5,0.5]
Switching gain	κT=0.014	λ=0.014	q_2h=0.017
Exponential coefficient	λ=5	q=5	q_1h=5
Others	ε=0.15,γ_1=0.1, α=2,η=20,γ_2=10	δ=0.15,φ=20 γ_2=10	α=0.5

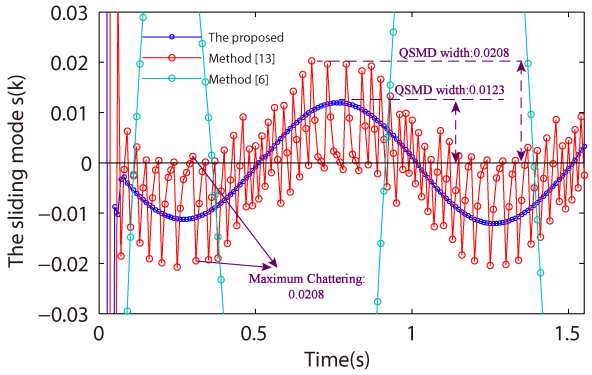

FIGURE 7. Partial enlarged drawing of Figure 6.

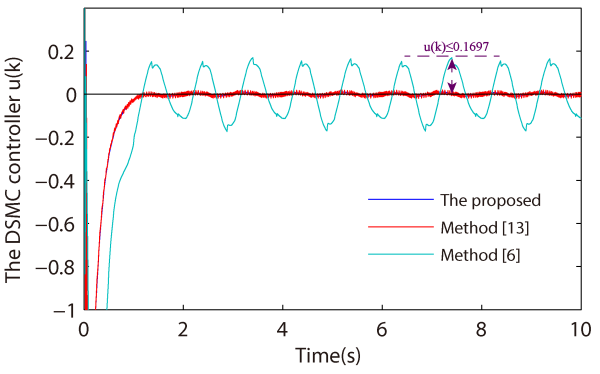

FIGURE 8. DSMC controller.

The error of the proposed, method [13] was $O(T^3)$ and the error of method [6] $O(T^2)$.

The maximum error of the proposed φ was 1.268×10^{-2}, maximum error of method [13] $\varphi_{[13]}$ 1.272×10^{-2}, and maximum error of method [6] $\varphi_{[6]}$ 1.676×10^{-2} (Fig. 5). Therefore, it was concluded that $\varphi \approx \varphi_{[13]} < \varphi_{[6]}$. At the same time, it should be pointed out that there was chattering on the disturbance estimation error curve of method [13].

Case II: To obtain the minimum QSMD width Δ_Φ, the adjustable switching gain of the three methods was selected to be the minimum. In view of (24) and Figure 5, settings were determined, with $\kappa T = 0.014$, $\lambda_{[13]} = 0.014$, and $q_2 T_{[6]} = 0.017$, where $\lambda_{[13]}$ was the switching gain of method [13], the $q_2 T_{[6]}$ respecting the switching gain of method [6]. In addition, according to [6], in which the sliding mode coefficient matrix C_e of method [6] should be [0.5, 0.5], large chattering was caused by a large C_e, and meanwhile, matrix C_e of the proposed method and method [13] was selected to be [5, 1]; the exponential coefficient of the three methods were the same $\lambda = 5$ and the others the same as the above. Generally, three controller parameters were selected as shown in Table 1.

Simulations of the sliding mode are shown in Figures 6 and 7, simulations of the controller shown in Figures 8 and 9, and simulations of system states shown in Figures 10 and 11.

a) System trajectories of method [6] lagged behind the proposed method and method [13] because of the smaller coefficient matrix C_e. Also, if this matrix was set to [5, 1], the switching function of method [6] that was related to the $s(k)$ caused a wider QSMD;
b) for the proposed and method [6], there was no chattering on the surface, while for method [13], the maximum value of chattering was ∼0.0208;
c) the QSMD width Δ_Φ of the proposed method was 0.0123, which was ∼0.0085 smaller than method [13], with $\Delta_{[13]} \approx 0.0208$ and method [6] leading to the maximum width, $\Delta_{[6]} \approx 0.126$;
d) the width of QSMD Δ_Φ was related to the upper bound of the disturbance estimation error $\varphi(k)$, such that the width Δ_Φ of the proposed method was smaller than method [6], and *Theorem 2(c)* has also proven here.

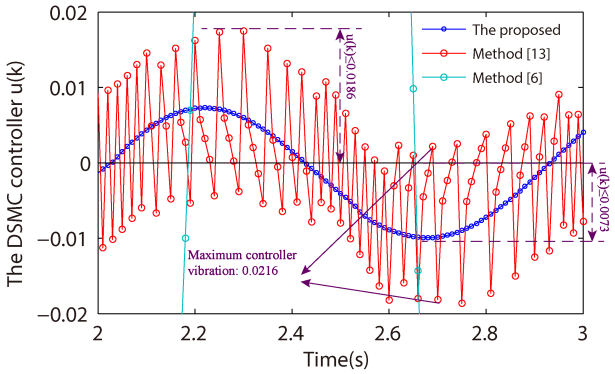

FIGURE 9. Partial enlarged drawing of the Figure 8.

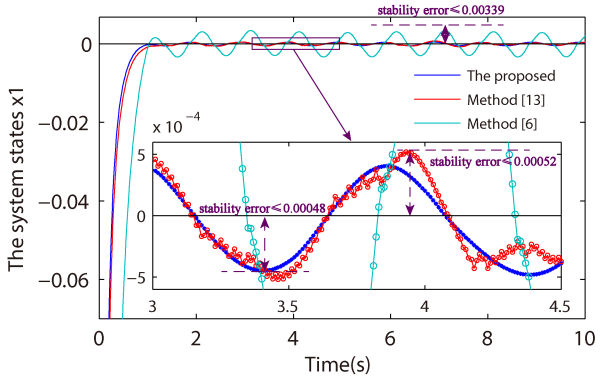

FIGURE 10. State *x1* trajectory.

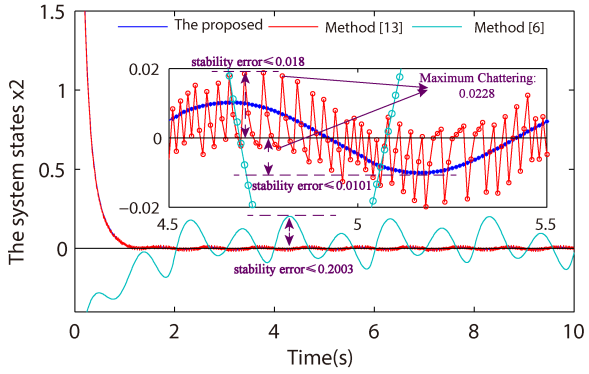

FIGURE 11. State *x2* trajectory.

In view of Figures 8–11, the following conclusions were drawn:

a) There was a high frequency vibration (∼0.0216) in the output of method [13] controller and the maximum amplitude $u_{[13]}$ was 0.0186, with both controllers of the proposed method and method [6] without high frequency vibration, $|u_p| < 7.3 \times 10^{-3}$, $|u_{[6]}| < 1.7 \times 10^{-2}$;

b) as the state *x1* stability error of method [6] was $|e_{x1[6]}| < 3.39 \times 10^{-3}$, the method [13] was $|e_{x1[13]}| < 5.2 \times 10^{-4}$, and the proposed method was $|e_{x1[p]}| < 4.8 \times 10^{-4}$, the comparison of the state stability error was $|e_{x1[6]}| > |e_{x1[13]}| > |e_{x1[p]}|$;

c) as the state *x2* stability error of method [6] was $|e_{x2[6]}| \leq 0.2003$, method [13] was $|e_{x2[13]}| \leq 1.8 \times 10^{-2}$, and the proposed method was $|e_{x2[p]}| \leq 1.01 \times 10^{-2}$, the comparison of the state stability error was $|e_{x2[6]}| > |e_{x2[13]}| > |e_{x2[p]}|$, and there was high frequency vibration on the state *x2* trajectory of method [13];

d) the high frequency vibration on the controller output or the state *x2* trajectory were reasons for chattering on the sliding surface, which affected system performance. The proposed method was able to eliminate chattering, thus improving control system accuracy.

TABLE 2. Simulation results.

Method	[6]	[13]	The proposed
Sliding mode chattering	≈0	≤0.0208	≈0
QSMD width	0.126	0.0208	0.0123
Controller vibration	≈0	≤0.021	≈0
State *x1* stability error	3.4×10^{-3}	5.2×10^{-4}	4.8×10^{-4}
State *x2* stability error	0.018	0.0228	0.0101

C. SUMMARY

Compared to method [6], the proposed method was able to produce a narrower QSMD width, smaller stability error, and improve the robustness with respect to external disturbances. And, compared to method [13], the proposed method was able to eliminate the chattering on the sliding surface, which caused high frequency vibrations of the controller. The simulation data is summarized in *Table 2*.

V. EXPERIMENTAL STUDIES

A. THE SHIPBORNE ELECTRO-OPTICAL SYSTEM

As a nonlinear system, the shipborne electro-optical control system is affected in practice by many factors. Changes in ship posture caused by ocean waves are main factors. When sailing on the sea, the platform is subjected to six-degrees-of-freedom (six-DOF) periodic motion resulting from interactions with ocean waves (Fig.12). Such ocean-generated motion contains translation (surge, sway, and heave) and rotation (roll, pitch, and yaw) [36]. And the six-DOF motion causes the optical axis to deviate from the target surface origin, with the pitch motor compensating for longitudinal axis deviation and azimuth motor for horizontal axis deviation of the target surface. Model uncertainties and torque ripple, and other nonlinear disturbances are also other interfering factors. SMC, as an effective approach to a robust control algorithm, was able to suppress the system parameter variations and the external nonlinear disturbances [18], with the specific contents described below.

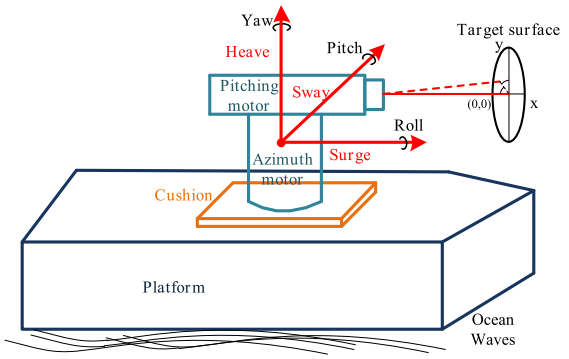

FIGURE 12. The shipborne electro-optical control system.

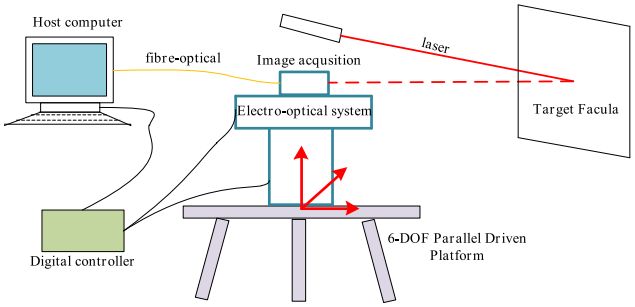

FIGURE 13. Experimental setup.

B. EXPERIMENTAL SETUP

The experimental setup is shown in Figures 13 and 14. During this experiment, the electro-optical plant was placed on a 6-DOF parallel driven platform (RX/YBT-6-500, Ruixin Technology Co., Ltd., Hong Kong, China) that could simulate the swaying motion of waves. Based on the real data obtained here, the shaking amplitude of optical axis did not exceed 5° and the frequency was less than 1 Hz under the conditions of level-five sea and large ships as carriers. Meanwhile, there was a laser facula on the target surface, which simulated the tracked target. The image processing system calculated the displacement after collecting this facula and fed it back to the digital control system driven by the controller signal. Attitude and other nonlinear disturbances were isolated by rotating the azimuth and pitch motors of the electro-optical system and optical axis stability was thus guaranteed. The physical of the experiment, as in Figure 14 described below.

System device selection and settings were as follows: the digital controller was composed of a DSP (TMS320F2812) and FPGA (Altera EP1C12Q240), with the DSP used to store the control algorithm, which calculated the control and attitude signals; the FPGA was used to receive and transmit command signals to achieve circuit logic control. Meanwhile, Code Composer Studio (CCS) software was used to develop the digital controller DSP, with control algorithms stored in the DSP to realize closed-loop control of the actuator. For the image system, the focal length of the camera (EoSens CL MC1362, MIKROTRON GmbH, Unterschleissheim, Germany) lens was set to 200 mm, the data acquisition frequency

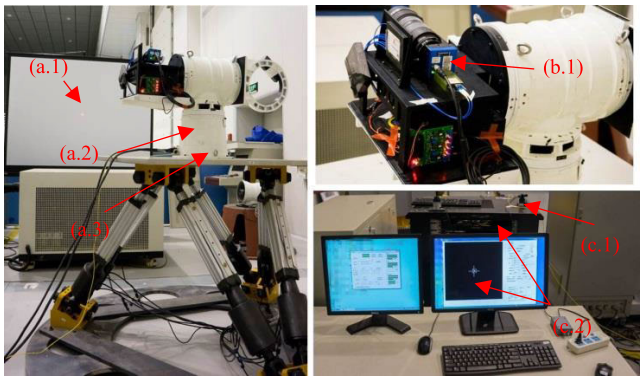

FIGURE 14. Photograph of the experimental platform a) Target facula (a.1), electro-optical system (a.2), and 6-DOF Parallel Driven Platform (a.3); b) Image acquisition system (b.1), and c) light source (c.1) and image display interface of the host computer (c.2).

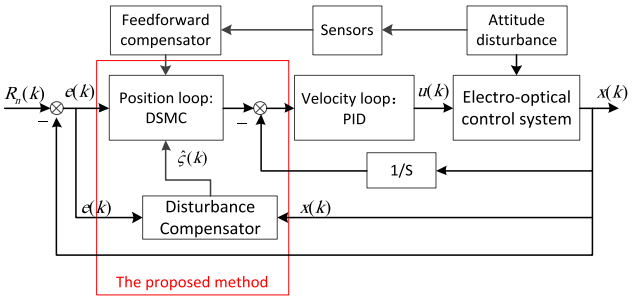

FIGURE 15. Structure of control algorithm for shipborne electro-optical platform.

to 0.1 kHz, and pixel size at 14×14 μm, which could be divided into 100 segments. The angle value of azimuth motor or pitch motor was obtained by encoder (RA26BEA115B05F, Renishaw Co., Inc, Gloucestershire, UK).

The structure of the control algorithm for the shipborne electro-optical platform is shown in Figure 15. There were two control algorithms used to accomplish the digital control system. One was a feedforward compensator, which received the attitude data of the inertial sensor; the disturbance components of the azimuth axis or pitch axis was calculated and compensated by the feedforward controller; and the attitude disturbance was isolated. The other was a nonlinear disturbance compensator composed of a velocity loop PID controller and position loop DSMC controller, such that the proposed DSMC with a disturbance compensator was able to suppress nonlinear disturbance and attitude disturbance residuals to ensure stability of the optical axis.

According to the structural diagram of the control system (Fig. 15), the closed-loop model was composed of the velocity loop controller, and the system model was the equivalent model of the position loop controller, in which the velocity loop controller was the PI controller, with P = 1.8, and I = 0.5. Therefore, the closed loop model of the velocity loop (41) was obtained by classical frequency domain model measurement method, and the model identification error was

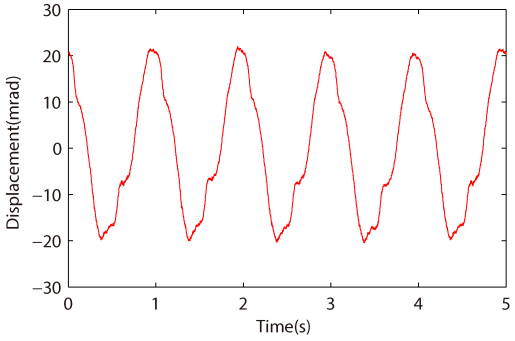

FIGURE 16. Optical axis deviation measurement.

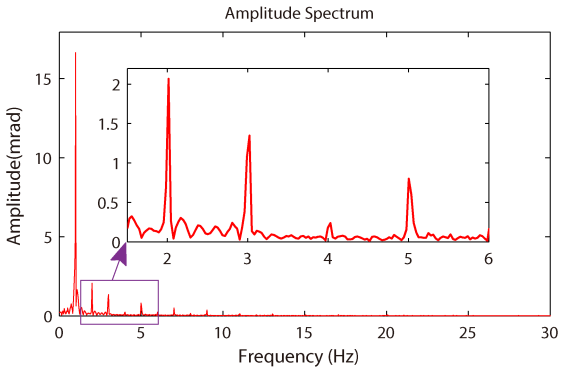

FIGURE 17. Amplitude spectrum of optical axis deviation.

a part of the system's nonlinear disturbance.

$$x(k+1) = (A + \Delta A)x(k) + (B + \Delta B)u(k) + B_f \rho(k)$$

$$A = \begin{bmatrix} 0.996 & -0.17 & -0.12 & -0.031 \\ 0.0098 & 0.9992 & -0.0006 & -0.0002 \\ 0 & 0.01 & 1 & 0 \\ 0 & 0 & 0.01 & 1 \end{bmatrix},$$

$$B = \begin{bmatrix} 0.0098 & 0 & 0 & 0 \end{bmatrix}^T \quad (41)$$

The controller parameters were selected as follows: $\varepsilon = 0.15$, $\gamma_1 = 0.1$, $\lambda = 5$, $\alpha = 2$, $\eta = 20$, and $\gamma_2 = 10$, the switching gain κT was selected to be 1.5; and the DSMC was the 4-order controller, such that the sliding mode coefficient matrix was set to [1, 3, 3, 1], which satisfied the Hurwitz polynomials *Lemma 1*). Therefore, taking azimuth motor control system as an example, experimental results were as follows below

C. EXPERIMENTAL CONCLUSION AND ANALYSIS

In the case of the 6-DOF parallel driven platform with 1 Hz shaking, the control system only retained the attitude disturbance feedforward compensator, and the remaining attitude disturbance showed that the comparison between the image acquisition optical axis deviation and estimation deviation curve (Fig. 16). It was obvious that the optical axis oscillated periodically around the coordinate origin at a frequency of 1 Hz with a maximum of ∼20 mrad affected by the attitude disturbance.

The amplitude spectrum of optical axis deviation is shown in Figure 17, which allowed conclusions to be obtained that the attitude perturbation at 1 Hz frequency was the main factor affecting optical axis stability and that its amplitude was ∼18.12 mrad. Also, there were other nonlinear disturbances at 2 and 3 Hz in the system, with the maximum amplitudes of 2.03 mrad.

To verify the effectiveness of the proposed DSMC controller (12), a laser beam pointing experiment was performed. Four control strategies, including the feedforward compensator plus PID controller, the feedforward compensator plus the DSMC controller that was method [6], method [13], or the proposed method, were adopted for comparative analysis in this experiment. The experimental results showed that the

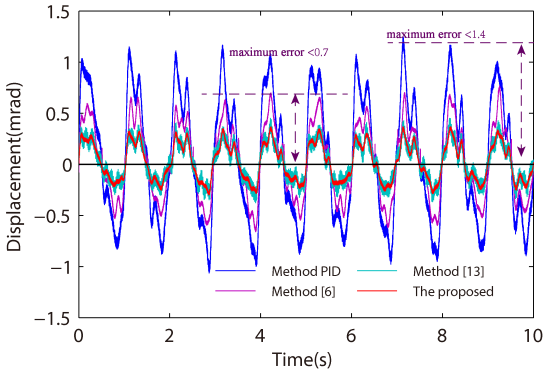

FIGURE 18. Laser beam pointing experiment state error.

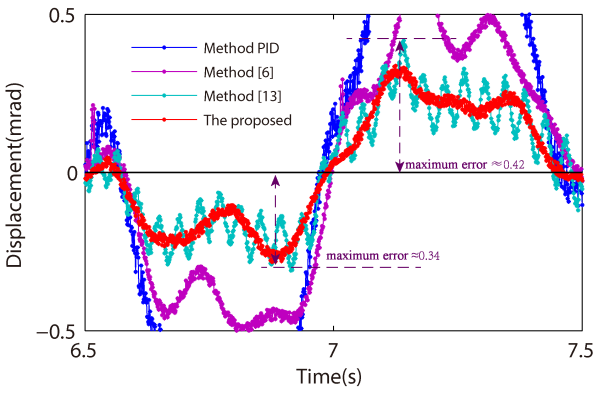

FIGURE 19. Partial enlarged drawing of Figure 18.

remaining attitude disturbance was suppressed by all four control strategies (Figs. 18 and 19). In view of these results, the maximum state error of the PID method was 1.38 mrad, which was greater than DSMC controller of method [6], at ∼0.68 mrad. The maximum error of the proposed method was the smallest, at ∼0.34 mrad, which was smaller than method [13], at ∼0.42 mrad. The disturbance isolation degree of method PID for uncompensated attitude disturbance was ∼23.2 dB, which was smaller than method [6], at ∼29.4 dB, while the disturbance isolation degree of method [13] and the proposed method was ∼34 dB.

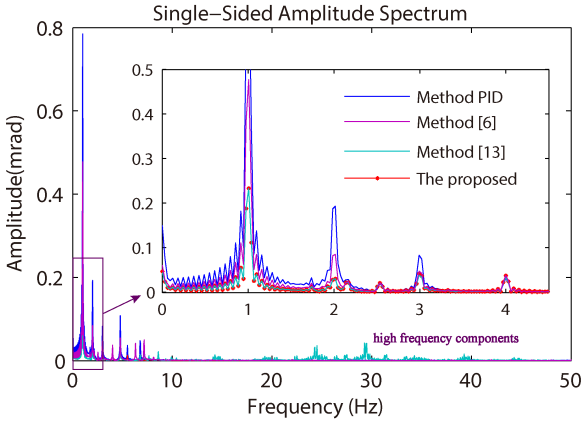

FIGURE 20. Amplitude spectrum of optical axis deviation.

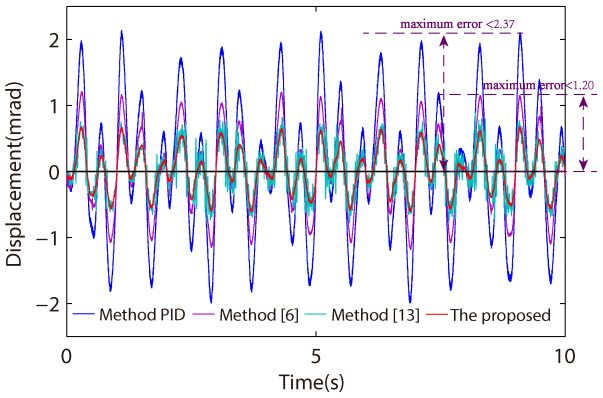

FIGURE 21. Facula tracking results at 2.5 Hz.

Figure 20 shows the amplitude frequency curve of Figure 18, indicating that the attitude disturbance of 1 Hz and the multiplication frequency disturbances caused by it were the main factors affecting system accuracy. The 1 Hz attitude disturbance amplitude of the proposed method or method [13] DSMC was ∼0.23 mrad, which was smaller than that of method [6], at ∼0.23 mrad, and the amplitude of the PID method at ∼0.79 mrad, which was the largest among the four methods. Meanwhile, it should be pointed out that there was a high frequency component in the state error of method [13], which was caused by sliding mode chattering and would have a serious impact on system stability. Therefore, compared with method [13], the proposed method was more reliable for the control system.

In the dynamic target equivalent tracking experiment, the laser transmitter was shaken by a 6-DOF parallel driven platform, which made the facula move sinusoidally at a frequency of 2.5 Hz with amplitude of 20 mrad on the target surface. The attitude disturbance of the level-five sea conditions was applied to the electro-optical system by the other 6-DOF parallel driven platform. The results showed that the remaining attitude disturbance and dynamic error were suppressed by all four control strategies (Figs. 21 and 22). In view of these results, the maximum state error of the PID method was ∼2.37 mrad, which was greater than the DSMC controller of method [6], at ∼1.20 mrad. The maximum state

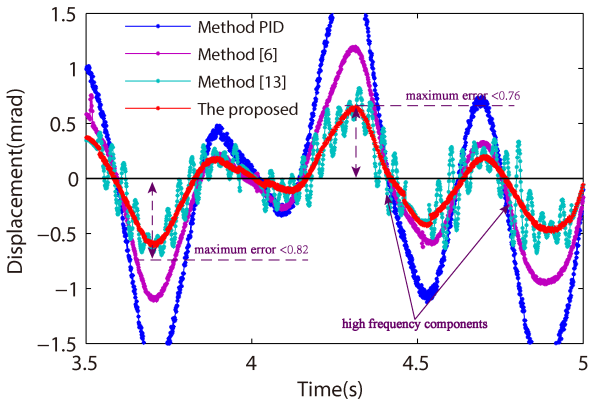

FIGURE 22. Partial enlarged drawing of the Figure. 21.

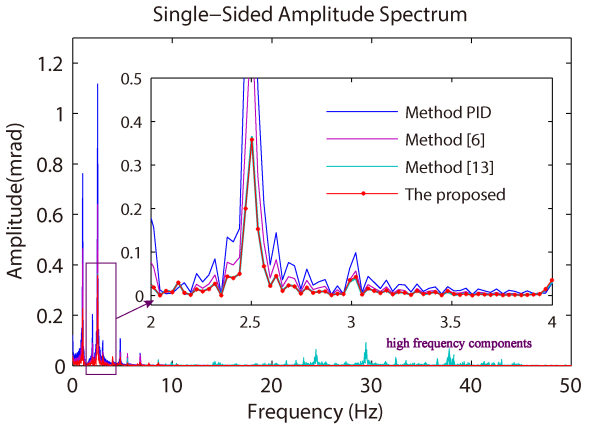

FIGURE 23. Amplitude spectrum of tracking error.

error of the proposed method was the smallest, at ∼0.76 mrad, which was smaller than method [13], at ∼0.82 mrad.

The amplitude frequency response curve clearly showed that the attitude disturbance of 1 Hz and the sinusoidal tracking error of 2.5 Hz were the two main factors affecting system accuracy (Fig. 23). From numerical analysis, the 1 Hz attitude disturbance amplitude and disturbance isolation degree were similar to the Figure 20 results. The amplitude of the PID method for the 2.5 Hz tracking error was ∼1.12 mrad, which was greater than that of method [6], at ∼0.74 mrad, and the amplitude of the proposed method or method [13] was ∼0.39 mrad. However, it should be pointed out that there were high frequency components in the state error of method [13], which was caused by sliding mode chattering and had negative influence on the control accuracy.

D. SUMMARY

Compared with the classical PID control algorithm, the three sliding mode controllers based on the RL achieved higher control accuracy and isolated the influence of attitude disturbance or dynamic error on the system. However, method [13] did not avoid the disadvantage of chattering in traditional sliding mode controllers, which can lead to a high frequency component in the state error. The proposed method

TABLE 3. Experimental results 1.

	Method	PID	[6]	[13]	The proposed
Static target	State error (mrad)	≤1.38	≤0.68	≤0.42	≤0.34
	1 Hz disturbance amplitude (mrad)	≈0.79	≈0.47	≈0.23	≈0.23
	High frequency component (Hz)	-	-	20-30	-
Dyna mic target	State error (mrad)	≤2.37	≤1.2	≤0.82	≤0.76
	2.5 Hz error amplitude (mrad)	≤1.12	≤0.74	≤0.39	≤0.39

TABLE 4. Experimental results 2.

	Method	Static target Tracking Accuracy	Dynamic target Tracking Accuracy
The proposed method compared with	Method [13](↗)	19%	7.3%
	Method [6](↗)	50%	37%
	Method PID(↗)	75%	65%

and method [6] were chatter-free methods, which were able to suppress chattering, and the QSMD width of the proposed method was $O(T^3)$, which was narrower than that of method [6], $O(T^2)$. Static target experimental data showed that the control accuracy of the proposed method was 19% higher than that of method [13] and 50% higher than that of method [6]. Dynamic target experimental data showed that the control accuracy of the proposed method was 7.3% higher than that of method [13] and 37% higher than that of method [6]. Experiment results are summarized in the *Tables 3* and *4*.

VI. CONCLUSION

In this paper, a new digital sliding mode controller based on a novel RL and n-order disturbance compensator was proposed for shipborne electro-optical systems. Mathematical calculations verified the convergence and stability of the proposed algorithm. Meanwhile, simulations showed that this proposed controller was able to suppress chattering on the sliding surface to avoid its influence on system stability and was robust to nonlinear disturbances, which also guaranteed a narrow QSMD. Finally, shipborne equivalent dynamic target tracking experiments were performed and the digital control-combined feedforward control with a SMC position loop and PID velocity loop control structure was adopted. The results, compared with the PID controller and other existing sliding mode controllers, showed that both the sliding mode and PID controllers isolated attitude disturbance, but the tracking error of the proposed method was the least of these approaches. Also, compared with existing method [13], the proposed method avoided the influence of sliding mode chattering on the system.

The research of a new reaching law algorithm with a simple structure and a narrower width to improve the present algorithm QSMD is the future work.

APPENDIX

a) This section was to prove the convergence of the n-order disturbance compensator shown in formula (10).

Proof: To prove the convergence of the disturbance compensator, the disturbance estimation error need only be proven to converge to a certain numerical range.

According to (10), the estimation error of disturbance compensator was expressed as

$$\varsigma(k) - \hat{\varsigma}(k) = \varsigma(k) - \varsigma(k-1) - \sum_{i=1}^{n} \alpha_i \cdot [\varsigma(k-i) - \varsigma(k-1-i)], \tag{a.1}$$

where it was obtained that

$$\begin{aligned}\sum_{i=1}^{n} \alpha_i \cdot [\varsigma(k-i) - \varsigma(k-1-i)] &= \alpha_1 [\varsigma(k-1) - \varsigma(k-2)] + \alpha_2 [\varsigma(k-2) - \varsigma(k-3)] \\ &\quad + \cdots + \alpha_n [\varsigma(k-n) - \varsigma(k-n-1)]\end{aligned} \tag{a.2}$$

In view of Assumption 2, if the change rate of the generalized uncertainty was bounded, there must be a small number δ that satisfies

$$-\delta \le \varsigma(m) - \varsigma(m-1) \le \delta \quad m = 2, 3, 4 \cdots, \tag{a.3}$$

and because of $\sum_{i=1}^{n} \alpha_i = 1$, equation (a.2) was expressed as

$$-\delta \le \sum_{i=1}^{n} \alpha_i \cdot [\varsigma(k-i) - \varsigma(k-1-i)] \le \delta. \tag{a.4}$$

According to (a.3) and (a.4), it was obtained that

$$\begin{aligned}-2\delta \le \varsigma(k) - \hat{\varsigma}(k) &= \varsigma(k) - \varsigma(k-1) \\ - \sum_{i=1}^{n} \alpha_i \cdot [\varsigma(k-i) - \varsigma(k-1-i)] &\le 2\delta.\end{aligned} \tag{a.5}$$

Above all, the estimation error (a.1) must converge in the $[-2\delta, 2\delta]$, therefore, the n-order disturbance compensator shown in formula (10) was converged.

b) This section was to prove that the inequality $\varphi/\kappa T \le \Gamma_2 < 1$ was well founded, where φ represents the upper bound of disturbance estimation error (14) and κT the switching gain of the proposed RL, and Γ_2 the state value of the functional equation $\Gamma_2(k)$ at a given time when the system entered into the QSMD.

Proof: At first, $\Gamma_2 < 1$ was proven.

As the system trajectories on the sliding surface, $|s(k)| \approx 0$ and $|e_1(k)| < 1$, then, $\Gamma_2(k)$ was expressed as

$$\Gamma_2(k) \approx \frac{|e_1(k)|^{2\alpha}}{|e_1(k)|^{\alpha} + 1}, \tag{b.1}$$

and thus, no matter the time, the equality $\Gamma_2 < 1$ was well founded. Next, the equality $\varphi/\kappa T \leq \Gamma_2$ was proven to be valid at $k = n$. According to (b.1), the equation $\varphi/\kappa T \leq \Gamma_2(k)$ was rewritten as

$$\kappa T \cdot |e_1(k)|^{2\alpha} - \varphi \cdot |e_1(k)|^{\alpha} + \varphi \geq 0, \tag{b.2}$$

with the formula (b.2) a quadratic inequality of one variable. Meanwhile, it was obtained that

$$\varphi^2 + 4\kappa T \cdot \varphi > 0. \tag{b.3}$$

There was a positive root $|e_1|$ satisfying the equation $\varphi\big/\kappa T = \Gamma_2(k)$ as

$$|e_1| = \frac{\varphi + \sqrt{\varphi^2 + 4\kappa T \cdot \varphi}}{2 \cdot \kappa T}. \tag{b.4}$$

The opening direction of inequality (b.3) was upward and, therefore, there must be a moment n in which the inequality $\varphi/\kappa T \leq \Gamma_2$ was valid.

Above all, the inequality $\varphi/\kappa T \leq \Gamma_2 < 1$ was well founded.

REFERENCES

[1] S. P. Garaba, D. Voß, J. Wollschläger, and O. Zielinski, "Modern approaches to shipborne ocean color remote sensing," *Appl. Opt.*, vol. 54, no. 12, pp. 3602–3612, 2015.

[2] Y. Zhang, S. Zhang, and Y. Qiao, "Feedforward control based on reference model disturbance observer of carrier-based optoelectronic theodolite," *Opt. Precis. Eng.*, vol. 54, no. 12, pp. 1213–1221, 2013.

[3] P. G. Lu and S. J. Shou, "High accuracy tracking technology and its application in ship-borne electro-optical system," *J. Appl. Opt.*, vol. 27, no. 6, Jun. 2006.

[4] T. Wang and S. Zhuang, "Study and experiment of ship movement simulation for free space laser communication," *Proc. SPIE*, vol. 7506, no. 3, pp. 251–253, Nov. 2009.

[5] Q. Wang, Y. Li, M. Diao, W. Gao, and F. Yu, "Coarse alignment of a shipborne strapdown inertial navigation system using star sensor," *IET Sci., Meas. Technol.*, vol. 9, no. 7, pp. 852–860, Oct. 2015.

[6] H. Du, X. Yu, M. Z. Q. Chen, and S. Li, "Chattering-free discrete-time sliding mode control," *Automatica*, vol. 68, pp. 87–91, Jun. 2016.

[7] B. Draženović, "The invariance conditions in variable structure systems," *Automatica*, vol. 5, no. 3, pp. 287–295, 1969.

[8] C. J. Fallaha, M. Saad, H. Y. Kanaan, and K. Al-Haddad, "Sliding-mode robot control with exponential reaching law," *IEEE Trans. Ind. Electron.*, vol. 58, no. 2, pp. 600–610, Feb. 2011.

[9] T. Yoshimura, "Adaptive sliding mode control for uncertain discrete-time systems using an improved reaching law," *Int. J. Model., Identificat. Control*, vol. 16, no. 4, pp. 380–391, Apr. 2012.

[10] X. Zhang, L. Sun, K. Zhao, and L. Sun, "Nonlinear speed control for PMSM system using sliding-mode control and disturbance compensation techniques," *IEEE Trans. Power Electron.*, vol. 28, no. 3, pp. 1358–1365, Mar. 2013.

[11] Z. P. Guo, C. M. Xie, and Y. J. Xiao, "Research of sliding mode control in electro-optical tracking system," *Adv. Mater. Res.*, vols. 756–759, pp. 403–406, Sep. 2013.

[12] W. Gao, Y. Wang, and A. Homaifa, "Discrete-time variable structure control systems," *IEEE Trans. Ind. Electron.*, vol. 42, no. 2, pp. 117–122, Apr. 1995.

[13] H. Ma, J. Wu, and Z. Xiong, "A novel exponential reaching law of discrete-time sliding-mode control," *IEEE Trans. Ind. Electron.*, vol. 64, no. 5, pp. 3840–3850, May 2017.

[14] W.-C. Su, S. V. Drakunov, and Ü. Özgüner, "An O (T^2) boundary layer in sliding mode for sampled-data systems," *IEEE Trans. Autom. Control.*, vol. 57, no. 5, pp. 482–485, Mar. 2000.

[15] V. Acary, B. Brogliato, and Y. V. Orlov, "Chattering-free digital sliding-mode control with state observer and disturbance rejection," *IEEE Trans. Autom. Control*, vol. 57, no. 5, pp. 1087–1101, May 2012.

[16] K. Abidi, J. X. Xu, and J. H. She, "A discrete-time terminal sliding-mode control approach applied to a motion control problem," *IEEE Trans. Ind. Electron.*, vol. 56, no. 9, pp. 3619–3627, Sep. 2009.

[17] Q. Xu, "Digital integral terminal sliding mode predictive control of piezoelectric-driven motion system," *IEEE Trans. Ind. Electron.*, vol. 63, no. 6, pp. 3976–3984, Jun. 2016.

[18] S. Li, H. Du, and X. Yu, "Discrete-time terminal sliding mode control systems based on Euler's discretization," *IEEE Trans. Autom. Control*, vol. 59, no. 2, pp. 546–552, Feb. 2014.

[19] Y. Wang, F. Yan, J. Chen, F. Ju, and B. Chen, "A new adaptive time-delay control scheme for cable-driven manipulators," *IEEE Trans. Ind. Informat.*, vol. 15, no. 6, pp. 3469–3481, Jun. 2019.

[20] Y. Wang, B. Li, F. Yan, and B. Chen, "Practical adaptive fractional-order nonsingular terminal sliding mode control for a cable-driven manipulator," *Int. J. Robust Nonlinear Control*, vol. 29, no. 5, pp. 1396–1417, Mar. 2019.

[21] Y. Wang, F. Yan, K. Zhu, B. Chen, and H. Wu, "A new practical robust control of cable-driven manipulators using time-delay estimation," *Int. J. Robust Nonlinear Control*, vol. 29, no. 11, pp. 3405–3425, Jul. 2019.

[22] Y. Wang, J. Chen, F. Yan, K. Zhu, and B. Chen, "Adaptive super-twisting fractional-order nonsingular terminal sliding mode control of cable-driven manipulators," *ISA Trans.*, vol. 86, pp. 163–180, Mar. 2019.

[23] S. Mobayen and F. Tchier, "A novel robust adaptive second-order sliding mode tracking control technique for uncertain dynamical systems with matched and unmatched disturbances," *Int. J. Control, Autom. Syst.*, vol. 15, no. 3, pp. 1097–1106, Jun. 2017.

[24] S. Mobayen and F. Tchier, "Composite nonlinear feedback integral sliding mode tracker design for uncertain switched systems with input saturation," *Commun. Nonlinear Sci. Numer. Simul.*, vol. 65, pp. 173–184, Dec. 2018.

[25] M. Afshari, S. Mobayen, R. Hajmohammadi, and D. Baleanu, "Global sliding mode control via linear matrix inequality approach for uncertain chaotic systems with input nonlinearities and multiple delays," *J. Comput. Nonlinear Dyn.*, vol. 13, no. 3, Mar. 2018, Art. no. 031008.

[26] A. Levant, "Homogeneity approach to high-order sliding mode design," *Automatica*, vol. 41, no. 5, pp. 823–830, May 2005.

[27] A. Bartoszewicz and P. Lesniewski, "Discrete time sliding mode control with reduced switching—A new reaching law approach," *Int. J. Robust Nonlinear Control*, vol. 26, no. 1, pp. 47–68, Jan. 2016.

[28] H. Ma, J. Wu, and Z. Xiong, "Discrete-time sliding-mode control with improved quasi-sliding-mode domain," *IEEE Trans. Ind. Electron.*, vol. 63, no. 10, pp. 6292–6304, Oct. 2016.

[29] S. Qu, X. Xia, and J. Zhang, "Dynamics of discrete-time sliding-mode-control uncertain systems with a disturbance compensator," *IEEE Trans. Ind. Electron.*, vol. 61, no. 7, pp. 3510–3512, Jul. 2014.

[30] X. Xia and A. S. I. Zinober, "Δ-modulated feedback in discretization of sliding mode control," *Automatica*, vol. 42, no. 5, pp. 771–776, May 2006.

[31] K. B. Devika and S. Thomas, "Power rate exponential reaching law for enhanced performance of sliding mode control," *Int. J. Control Automat. Syst.*, vol. 15, no. 6, pp. 2636–2645, Dec. 2017.

[32] H. Hou and Q. Zhang, "Novel sliding mode control for multi-input–multi-output discrete-time system with disturbance," *Int. J. Robust Nonlinear Control*, vol. 28, no. 8, pp. 3033–3055, May 2018.

[33] Y. Niu, D. W. C. Ho, and Z. Wang, "Improved sliding mode control for discrete-time systems via reaching law," *IET Control Theory Appl.*, vol. 4, no. 11, pp. 2245–2251, Nov. 2010.

[34] J. Li, H. Su, Y. Zhang, Z. Wu, and J. Chu, "Chattering free sliding mode control for uncertain discrete time-delay singular systems," *Int. J. Robust Nonlinear Control*, vol. 15, no. 1, pp. 260–269, Jan. 2013.

[35] B. L. Cong, Z. Chen, and X. D. Liu, "On adaptive sliding mode control without switching gain overestimation," *Int. J. Robust Nonlinear Control*, vol. 24, no. 3, pp. 515–531, Feb. 2014.

[36] G. Chang, M. Li, J. Xie, L. Zhang, C. Yu, and Y. Ji, "Ocean surface current measurement using shipborne HF radar: Model and analysis," *IEEE J. Ocean. Eng.*, vol. 41, no. 4, pp. 970–981, Oct. 2016.

[37] C. Kwan, "Further results on variable output feedback controllers," *IEEE Trans. Autom. Control*, vol. 46, no. 9, pp. 1505–1508, Sep. 2001.

[38] A. J. Fossard and T. Floquet, "Introduction: An overview of classical sliding mode control," In *Sliding Mode Control in Engineering*, vol. 11, W. Perruquetti and J. P. Barbot, Eds. New York, NY, USA: Marcel Dekker, 2002.

JIANQIANG ZHANG was born in Shandong, China, in 1992. He received the B.E. degree from Shandong University, China, in 2015. He is currently pursuing the joint Ph.D. degree with the University of Chinese Academy of Sciences and the Changchun Institute of Optics, Fine Mechanics and Physics, Chinese Academy of Sciences, China. His research interests include laser communication control systems, shipborne electro-optical systems, motor control technology, model identification technique, digital sliding-mode control, and the uncertain systems.

YONGKAI LIU was born in Heilongjiang, China, in 1989. He received the B.E. and M.S. degrees from the Harbin Institute of Technology, China, in 2012 and 2014, respectively. He is currently pursuing the joint Ph.D. degree with the University of Chinese Academy of Sciences and the Changchun Institute of Optics, Fine Mechanics and Physics, Chinese Academy of Sciences, China. His research interests include the application of adaptive optics in free-space optic communication, high-precision laser tracking and control, and digital control based on DSP and FPGA.

FENGJING ZHANG was born in Changchun, China, in 1979. She received the master's degree from the Changchun University of Science and Technology, China, in 2007. She is currently with the Aviation University of Air Force. Her research interests include electro-optical systems and digital image processing.

SHIJIE GAO was born in Jilin, China, in 1979. He received the B.E. degree from the Harbin University of Science and Technology, and the M.S. and Th.D. degrees from the Changchun Institute of Optics, Fine Mechanics and Physics, Chinese Academy of Sciences, China, in 2006 and 2015, respectively. Since 2006, he has been with the Changchun Institute of Optics, Fine Mechanics, and Physics, Chinese Academy of Sciences, China, where he is currently a Professor with the Department of Optical-Electronic Detection. His research interest includes optical communication technology. He has authored or coauthored more than 15 publications in his main research area.

CHENGSHAN HAN was born in Jilin, China, in 1972. He received the B.E. degree from the Jilin University of Technology, in 1993, and the M.S. and Th.D. degrees from the Changchun Institute of Optics, Fine Mechanics and Physics, Chinese Academy of Sciences, China, in 1998 and 2005, respectively. He has been with the Changchun Institute of Optics, Fine Mechanics, and Physics, Chinese Academy of Sciences, China, where he is currently the Director of the Space Optics Department II. His research interests include control theory and applications and the control technology of space camera. He has authored or coauthored more than 30 publications in his main research areas.